Carrier generation and carrier determination in dipyridyldiketopyrrolopyrrole-based H_2 gas sensors

H. Takahashi and J. Mizuguchi[a)]
Department of Applied Physics, Graduate School of Engineering, Yokohama National University, 240-8501 Yokohama, Japan

(Received 6 January 2006; accepted 8 June 2006; published online 4 August 2006)

Operation mechanism of dipyridyldiketopyrrolopyrrole (DPPP)-based H_2 sensor has been investigated with special attention to the electric-field-assisted dissociation of H_2 in the presence of Pd or Pt, as well as the carrier generation and carrier determination. H_2 is found to dissociate exponentially with an increase of the electric field above 10^{2-3} V/cm as monitored by an electric current. The dissociation is greatly enhanced by the presence of DPPP which serves as a proton acceptor due to its pyridyl-N atom. The detection of H_2 starts with dissociation of H_2, followed by protonation of atomic hydrogen (H) at the N atom of the pyridyl ring of DPPP, ending up with a release of an electron which contributes to the electrical conduction: H+pyridyl ring $\rightarrow$protonated pyridyl ring $(N^+-H)+e'$. The electron conduction is confirmed by the Seebeck effect. Judging from the above process, the atomic hydrogen is pictured as an electron donor. However, the present doping is rather characterized by an instantaneous one, since the extent of doping depends on the ambient H_2 concentration. © *2006 American Institute of Physics*. [DOI: 10.1063/1.2227215]

I. INTRODUCTION

Diketopyrrolopyrroles [DPP: Fig. 1(a)] are industrially important red pigments used widely in painting and imaging industries,[1] as well as for liquid crystal display (LCD) color filters.[2] Thionated derivatives of DPP, as obtained by replacing of the carbonyl oxygen atoms by sulfur atoms, have also attracted attention as a material for photoconductors for laser printers[3–5] as well as for optical disks on the basis of GaAsAl laser diodes.[6]

Quite recently, we have reported an application of DPPs for H_2 gas sensors, utilizing a high proton affinity of dipyridyl DPP [DPPP: Fig. 1(b)] derivative.[7] DPPP is known to exhibit a remarkable color change [vivid red to violet: Fig. 2(a)] upon exposure to the vapor of nitric acid, also accompanied by a drastic reduction in electrical resistivity by five orders of magnitude [Fig. 2(b)].[8] The present outstanding effect is found to occur due to protonation at the N atom of the pyridyl ring and indicates that DPPP can be used as a material for acid sensors. However, in view of the advent of fuel cells in the near future, we tried to transform it into a H_2 gas sensor with the following idea. We believed that H_2 can dissociate into atomic hydrogens assisted by a high electric field in the presence of Pd or Pt. Then, the atomic hydrogen (H) protonates DPPP at the N atom to release an electron that contributes to the electrical current: H+pyridyl ring $\rightarrow$protonated pyridyl ring $(N^+-H)+e'$. We have integrated these functions into interdigital electrodes as shown in Fig. 3(a) where a trace of Pd or Pt is directly sputtered onto indium tin oxide (ITO) electrodes in the form of islands (ca. 3 Å) [Fig. 3(b)].[7] Then, DPPP layer is applied by vacuum evaporation (ca. 300 Å). H_2 is first adsorbed on the surface of DPPP and diffuses into the bulk where H_2 encounters sputtered Pd. Then, H_2 dissociates into hydrogen atoms under a high electric field: $H_2(ads) \rightarrow H(ads)+H(ads)$. At this moment, the N atom of the pyridyl ring of DPPP (strong proton acceptor) captures the proton by releasing an electron. The sensor exhibits a remarkable reduction of resistivity by two orders of magnitude even under 0.05% H_2.

In spite of the above excellent performance, little is known about the detailed operation mechanism, especially the effect of a high electric field on the dissociation of H_2 into protons, as well as the carrier generation and carrier determination. For this reason, an attempt was made in the present investigation to gain more insight into the sensing process, especially carrier generation and carrier determination by means of a thermoelectric power method based upon the Seebeck effect.[9,10] In parallel, the carrier generation process by means of the vapor of nitric acid is also discussed on the basis of correlation between electrical resistivity and spectral changes.

II. EXPERIMENT

A. Preparation of DPPP

DPPP was synthesized according to the method described in Ref. 11 and purified three times by sublimation, using a two-zone furnace.[12]

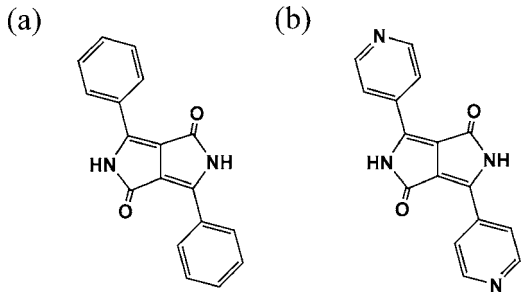

FIG. 1. Molecular conformation of DPP and DPPP.

[a)]Electronic mail: mizu-j@ynu.ac.jp

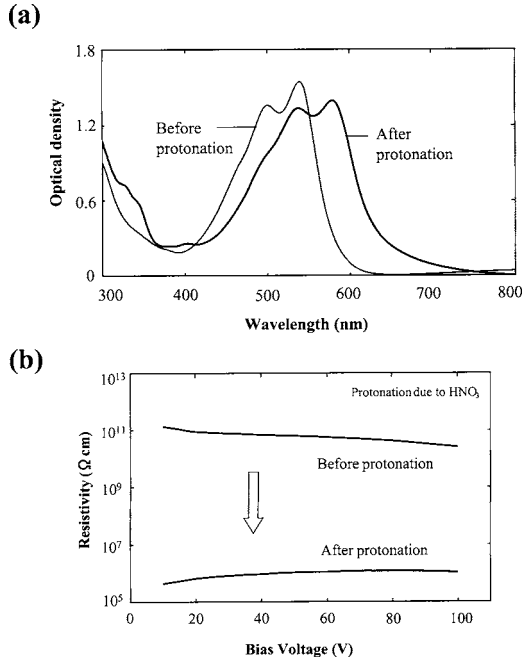

FIG. 2. Protonation at the N atom of DPPP with the vapor of nitric acid: (a) change in absorption spectra and (b) change in electrical resisitivity.

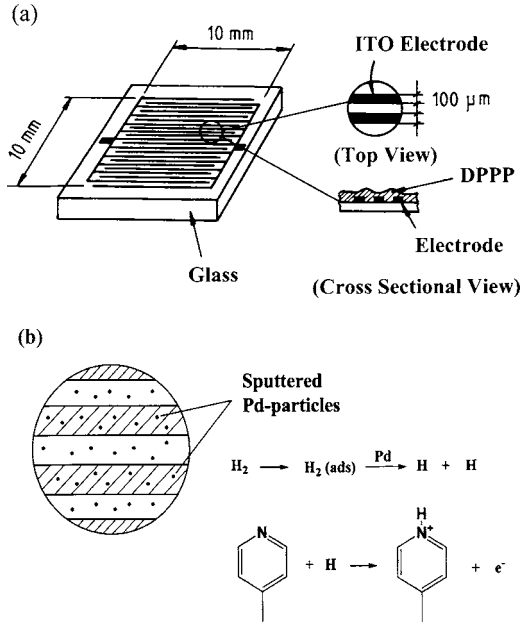

FIG. 3. Structure of the H_2 gas sensor: (a) interdigital electrodes and (b) magnified picture of the Pd-sputtered electrodes.

B. Experimental setup for measurements of the Seebeck effect

Figure 4 shows the experimental setup for measurements of the Seebeck effect.[9,10] This method evaluates the thermoelectric power which appears between hot and cold ends of a material. The hot end is made by a soldering iron maintained at 100 °C while the cold end is the ITO electrode at room temperature. If the potential of the hot end is positive, then the carrier is electrons. Similarly, if the potential is negative, the charge carrier is due to holes.

C. Sample preparation

For the study of the field effect on the H_2 dissociation, Pd or Pt was sputtered directly onto the interdigital ITO electrodes [Fig. 3(b)] by a sputter equipment (E-1030 ion sputter from Hitachi Corporation) in such a way as to form islands of Pd or Pt (cell structure: ITO/Pd/ITO). Then, the current caused by dissociation of H_2 into protons was measured under 100% H_2 as a function of an electric field from 10^1 to 10^5 V/cm.

Since the measurement of the Seebeck effect requires a temperature gradient along the direction of the film thickness (Fig. 4), the DPPP layer in the H_2 gas sensor was prepared thicker (about 1200 Å) than the standard one (about 300 Å). Because of this, the present sensor was much less sensitive by about two to three orders of magnitude than the standard one. This is a trade-off for meaningful measurements of the Seebeck effect. Evaporated DPPP is well crystallized which corresponds to phase I.[13] Besides the H_2 gas sensor, we prepared two additional samples: evaporated DPPP and evaporated/protonated DPPP (i.e., a model substance of the H_2 gas sensor). DPPP was vacuum-deposited onto an ITO/glass substrate to the thickness of about 1200 Å. Protonation was carried out by exposing evaporated DPPP to the vapor of nitric acid for 1 min.

In order to study the correlation between carrier formation and color changes of evaporated/protonated DPPP with nitric acid, simultaneous measurements of both electrical resisitvity and spectral changes were made for four variously vapor-treated samples. DPPP was evaporated onto interdigital ITO electrodes (about 300 Å; cell structure: ITO/Pd/ITO). The film was then exposed to the vapor of nitric acid for 8, 12, 15, and 20 s and then dried at room temperature for 10 min. After that, the electrical resistivity was measured while monitoring the absorption spectrum.

D. Molecular orbital (MO) calculations

The geometry of initial DPPP as well as mono- and diprotonated DPPPs was optimized by means of the AM1 Hamiltonian of MOPAC program package.[14] Then, the spectroscopic calculations for each state were made on the basis of the INDO/S Hamiltonian.[14]

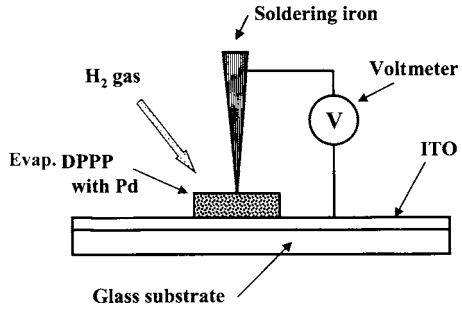

FIG. 4. Experimental setup for measurements of the Seebeck coefficient.

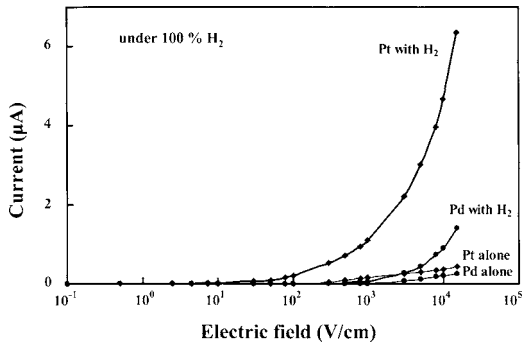

FIG. 5. Electric field dependence on the dissociation of H_2 into protons.

III. RESULTS AND DISCUSSION

A. Field dependence of the H_2 dissociation

Figure 5 shows the current versus applied electric field for samples of ITO/Pd/ITO and ITO/Pt/ITO in the absence or presence of 100% H_2. No noticeable current was recognized in the absence of H_2 in both samples. However, the current due to H_2 dissociation builds up exponentially in the presence of H_2 above the electric field of about 10^2 V/cm in Pt and about 10^3 V/cm in Pd. The present result clearly indicates that the electric-field-assisted dissociation of H_2 occurs even in the solid state and that the interdigital electrodes with Pd or Pt is quite effective to facilitate the H_2 dissociation into protons, especially in Pt. It is also important to note that the dissociation is greatly enhanced by the presence of a proton acceptor (i.e., DPPP) by two to three orders of magnitude.[7] Actually, this is the structure of the H_2 gas sensor shown in Fig. 3.

B. Carrier determination

Figure 6 shows the thermoelectric power versus time that appears between the hot and cold ends of the H_2 gas sensor under 100% H_2, for evaporated DPPP, evaporated/protonated DPPP and the H_2 sensor based upon DPPP. As soon as the contact is made between the soldering iron and the H_2 sensor, a positive potential of about 0.2 mV appears at the hot end. The moment H_2 is introduced, a small positive potential of about 0.04 mV relative to DPPP appears at the hot end, indicating that the charge carrier is due to electrons. The present result directly supports the operation principle of the H_2 gas sensor shown in Fig. 3(b): $H_2 \rightarrow H+H$, and H +pyridyl ring $\rightarrow$ protonated pyridyl ring $(N^+-H)+e'$. The atomic hydrogen is pictured here as an electron donor. However, the present doping depends on the ambient H_2 concentration. Therefore, the process is rather characterized by an instantaneous doping.

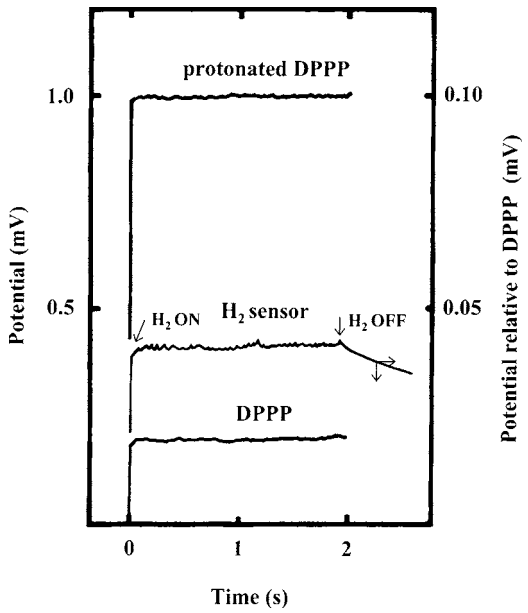

FIG. 6. Themoelectric power observed along the direction of the temperature gradient for three samples: H_2 gas sensor under 100% H_2, evaporated DPPP, and evaporated/protonated DPPP.

TABLE I. Molecular orbital calculations for initial, monoprotonated and diprotonated states of DPPP.

Molecular state	Heat of formation (kJ/mol)	Optical absorption band	
		Λ (nm)	f[a]
Initial	318.3	404.0	0.680
Monoprotonated	959.6	451.1	0.461
Diprotonated	1778.7	461.8	0.717

[a]Oscillator strength.

Similarly, positive potentials were also observed in samples of evaporated DPPP and evaporated/protonated DPPP, indicating that the charge carriers are electrons. However, one should note that the thermoelectric power of evaporated/protonated DPPP is much larger than that of evaporated DPPP. This suggests that a great deal of charge carriers are generated by protonation with the vapor of nitric acid.

C. Stability and color of the initial, mono-, and diprotonated states as deduced from MO calculations

Table I details the result of MO calculations for the heat of formation and absorption bands for the initial, mono-, and diprotonated states. As judged from the heat of formation, the initial state is quite stable (318.3 kJ/mol); whereas the heat of formation increases significantly due to monoprotonation (959.6 kJ/mol) and furthermore due to diprotonation (1778.7 kJ/mol). This indicates that the mono- and diprotonated states are not so stable as that of the initial state and that the protonated states show a tendency to give up a proton (or protons) to return to the initial state.

All absorption bands shown in Table I are due to "highest occupied molecular orbital"/"lowest unoccupied molecular orbital" π-π^* transitions. The band in the initial state appear at the shortest wavelength and is then displaced toward longer wavelengths upon protontion. The bathochromic shift is more striking in diprotonation than in monoprotonation. The tendency of the bathochromic shift due to protonation is in good agreement with experiment shown in Fig. 2(a) where the sample is diprotonated as shown by our element analysis: DPPP/$(HNO_3)_2$.[8] The calculated wavelengths of the absorption bands show the correct trend, but the absolute values are not similar to the experimental values. This is due mainly to the semiempirical program itself[14] in which the

parameters are optimized by using small molecules. This underestimates, in general, the absorption band toward shorter wavelengths. Furthermore, an additional bathochromic shift occurs, on going from solution to the solid state, due to interactions between transition dipoles in DPP compounds.[15]

D. Protonation of the N atom of the pyridyl ring in DPPP as caused by the vapor of nitric acid or H_2

Up to now, we believed that evaporated/protoanted DPPP is the model substance of the H_2 gas sensor and that the operation of the H_2 gas sensor is, in principle, based upon the protonation behavior of DPPP associated with the change in color and resistivity due to the vapor of nitric acid. However, we point out here some differences between them. In H_2 gas sensors, the resistivity reduces quite significantly when H_2 is introduced. However, no color change is visually recognized in the DPPP layer during this process.[7] Furthermore, when H_2 is switched off, the sensor signal comes back to the initial state in 5 min due to desorption of H_2 from the surface: $H^+ + e' \rightarrow 1/2\ H_2(\text{ads}) \rightarrow 1/2 H_2(\text{gas})$.[7] That is, the sensor is reversible, although the return process is rather slow. On the contrary, vapor treatment with nitric acid brings about immediately the color change from vivid red to violet [Fig. 2(a)], and the violet color remains intact unless the sample is heated above ca. 200 °C or washed with water.[8]

We discuss first why the sensor is reversible, and then the problem of the reduction in resisitivity with no color change will be treated in the next section. The decay process of the sensor signal when H_2 is switched off seems to be closely related to the stability of the protonated state. As seen from Table I, the heat of formation increases considerably with mono- and diprotonation, indicating that the protonated state is more unstable than the initial one and thus inclines to return to the initial state by spontaneously releasing protons, ending up with the formation and desorption of H_2 as described above. Then, we consider why protonation with nitric acid induces a color change immediately from red to violet and the color remains unchanged. First of all, we call attention to the fact that the protonated layer has a composition of $DPPP/(HNO_3)_2$ according to our element analysis reported previously.[8] The monoprotonated state ($DPPP^+ - H$) as well as the diprotonated one ($DPPP^{2+} - H_2$) are unstable as shown in Table I. However, these cations are stabilized by the counter anion of NO_3^- in the solid state. Therefore, the violet color remains intact unless the sample is heated above ca. 200 °C or washed with water.[8]

E. Correlation between color change and carrier formation

Figure 7(a) shows the spectral change as a function of time of vapor treatment with HNO_3 from 0 to 20 s. The vapor treatment for 8 s brings about an absorption shoulder around 580 nm, and this grows up to an absorption band with further vapor treatment. No more spectral change is recognized after the treatment time over 15 s. Figure 7(b) shows the resitivity change as a function of time after vapor treatment for the corresponding samples used for measurements of the absorption spectra. The resistivity value at time

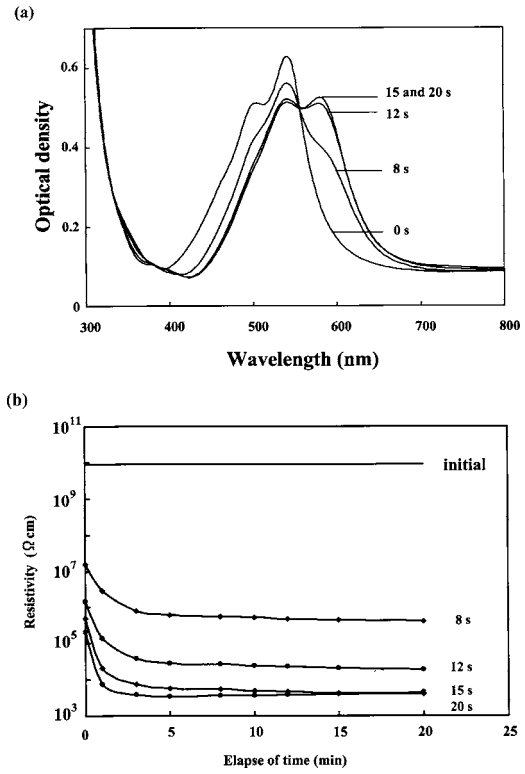

FIG. 7. (a) Spectral change due to protonation with the vapor of nitric acid as a function of vapor treatment time and (b) resistivity decrease in protonated DPPP as a function of time after vapor treatment.

zero is the value of the sample which has been vapor treated and then dried for 10 min. (This dry process is absolutely necessary, because the wet sample gave rather irreproducible results. In addition, the evaporated film came off sometimes during the measurement.) It is evident that some carriers are formed upon protonation, as well as the subsequent dry process as shown by the reduction in resistivity from the initial value. We call this the first doping process. Then, it is very interesting to note that the resitivity further decreases by one to two orders of magnitude with elapse of time after vapor treatment [Fig. 7(b)]. It is also important to mention that no spectral change is observed during this period. That is, the reduction in resistivity at this moment occurs quite irrespective of the color change. This indicates that additional carriers are formed gradually after vapor treatment. We refer to this process as the second doping. In summary, the generation of charge carriers proceeds in two steps. The first step occurs immediately upon vapor treatment and in the subsequent dry process, giving rise to both spectral change and carrier doping. On the other hand, the second doping takes place without accompanying any spectral change.

At this point, it should be remembered that the composition of protonated DPPP with nitric acid is $DPPP/(HNO_3)_2$ as shown in route I in Fig. 8.[8] Judging from this composition, the color change occurs, but no carrier is expected to appear. However, we should also take into account the important fact that a significant conductivity appears in semiconductors as a result of even a small doping,[10] for example, less than 10^{-3}% doping that creates a carrier concentration of about $10^{17}/\text{cm}^3$: whereas no color change occurs at this doping

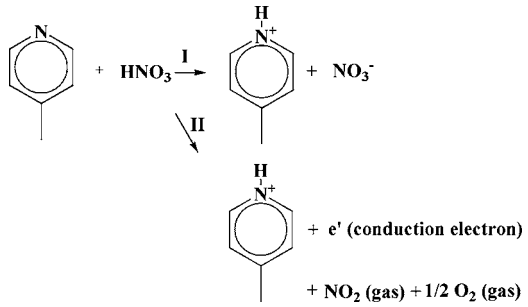

FIG. 8. Proposed protonation mechanism: (I) with color change but without carrier formation and (II) with carrier formation but without color change. Route II corresponds to a doping level which is too low to give a color change.

level. That is, the color generation normally requires a much higher concentration in the order of a few percents. These considerations allow us to assume that the carrier generation proceeds presumably as shown in route II in Fig. 8, releasing one electron and evolving NO_2 and O_2. In the first doping process, route I (i.e., color generation) prevails together with a small portion of carrier formation (route II). On the contrary, in the second doping process, the carrier generation (route II) is the major process with little color change (route I).

In short, the mechanism of the charge carrier formation due to H_2 in the H_2 gas sensor is slightly different from that of DPPP due to the vapor of nitric acid, although the charge carriers are electrons in both processes (see the Seebeck experiment).

Since the charge carriers are determined to be electrons, the frequency response of the sensor has been studied in order to optimize the sensor operation. The result is given in the Appendix.

IV. CONCLUSIONS

The conclusions drawn from the present study can be summarized as follows. Application of a high electric field is found to be quite effective to assist the dissociation of H_2 into protons. The charge carriers are determined to be electrons for the H_2 sensors based upon DPPP, as well as for evaporated DPPP and evaporated/protonated DPPP. The mechanism of the charge carrier formation in the H_2 gas sensor is slightly different from that of DPPP due to the vapor of nitric acid, although the charge carriers are electrons in both processes. In evaporated/protonated DPPP with nitric acid, protonation brings about primarily the color change from vivid red to violet and secondarily carrier generation. However, this is not yet conclusive and requires further investigation.

APPENDIX: FREQUENCY RESPONSE OF THE SENSOR

In our previous report,[7] the H_2 gas sensor was driven with DC (direct current). Because of this, the electrons released from H_2 are found to gradually accumulate at the interface between DPPP and ITO to form a space charge which blocks electron flow. Therefore, the polarity of the

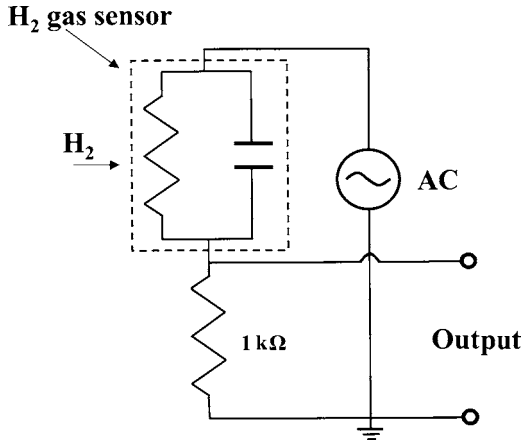

FIG. 9. ac drive circuit for measurements of the frequency response of the H_2 gas sensor.

electrodes should be changed before the formation of the space charge. This suggests that alternating current (ac) drive provides a better performance. For this reason, a frequency response of the H_2 gas sensor has been studied.

Figure 9 shows the measuring circuit for the frequency response. The H_2 gas sensor is pictured as composed of a resistance and a condenser in parallel. A load resistance of 1 kΩ was connected in series with the gas sensor. Frequency response was measured with a voltage of 14 V_{eff} (effective voltage) of the sine wave in the range between 10 and 2×10^5 Hz.

The interdigital ITO electrodes whose intervals are 50 and 100 μm were prepared by photolithographic technique [see Fig. 3(a)]. Then, Pd was directly applied onto the interdigital electrode by sputtering in the form of islands so as to avoid contacts between two electrodes. After that, a thin layer of DPPP (300 Å) was applied by vacuum evaporation.

Since the H_2 gas sensor can be regarded as consisting of a resistance and a condenser as shown in Fig. 9, the current which flows through the circuit under H_2 includes two components: one is due to H_2 (i.e., real current, or reaction current) and the other is due to charge/discharge of the capacitance (i.e., displacement current). In order to separate these two components, the frequency response of the interdigital electrode with DPPP was also measured and used as the reference.

Figure 10 shows the frequency response of the samples for electrode intervals of 50 and 100 μm in the presence or

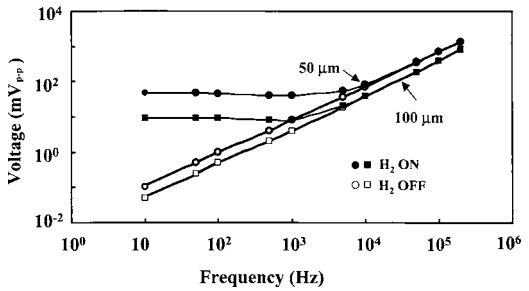

FIG. 10. log-log plot of the signal output vs frequency. Two types of electrode intervals were used, 50 and 100 μm (see Fig. 3). Measurements were made in the absence or presence of 100% H_2.

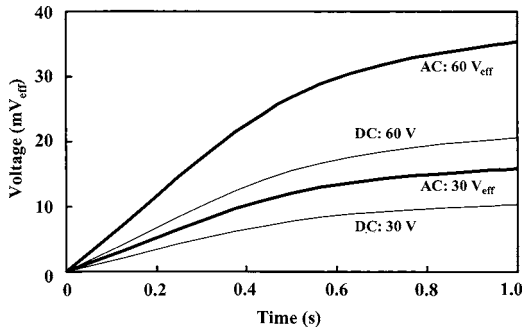

FIG. 11. Buildup of the sensor signal under 100% H_2 with the operation of dc and ac. Cell structure: ITO/Pd/DPPP/ITO.

absence of 100% H_2 gas. In both samples with 50 and 100 μm electrodes, the output voltage of the sensor is larger in the presence of H_2 in the frequency range from 10 to 5 kHz as compared with that of those in the absence of H_2. This difference is attributed to the real current (i.e., reaction current) due to H_2. The difference becomes larger as the frequency is lowered towards dc while it becomes smaller with higher frequencies. Then, no more difference is recognized in both samples above 5 and 10 kHz for the electrodes with 100 and 50 μm, respectively, where only the displacement current prevails due to the condenser component of the sample. This indicates that the reaction rate for the detection of H_2 is too slow to follow the alternating electric field. These results lead us to operate the sensor in the frequency region between 10 and 500 Hz.

Figure 11 shows the buildup of the signal output under the operation of dc and ac in the presence of H_2. ac voltages are expressed here in effective values. It is remarkable to note that the ac 30 V_{eff} gives a higher output than the dc 30 V by a factor of 1.5. The output voltage is further enhanced by a factor of 1.75 with ac 60 V_{eff} as compared with that of dc 60 V. These results allow us to conclude that ac drive provides basically a better performance of the sensor by a factor of 1.5–1.75. The enhancement of the output signal can largely be attributed to the obviation of the polarization effect due to dc drive at the interface between electrode and DPPP.

In conclusion, the H_2 gas sensor is found to enhance the output signal under ac operation by a factor of about 1.5–1.75 in the frequency range between 10 and 500 Hz, as compared with dc drive.

[1]W. Herbst and K. Hunger, *Industrial Organic Pigments*, 2nd ed. (VCH, Weinheim, 1997), pp. 489–496.
[2]K. Ichimura, S. Kobayashi, T. Komatsu, and S. Okazaki, Japan Patent No. Heisei 4-37987 (filed June 23, 1992).
[3]J. Mizuguchi and A. C. Rochat, J. Imaging Sci. **32**, 135 (1988).
[4]J. Mizuguchi and S. Homma, J. Appl. Phys. **66**, 3104 (1989).
[5]J. Mizuguchi, J. Appl. Phys. **66**, 3111 (1989).
[6]J. Mizuguchi, G. Giller, and E. Baeriswyl, J. Appl. Phys. **75**, 514 (1994).
[7]H. Takahashi and J. Mizuguchi, J. Electrochem. Soc. **152**, H69 (2005).
[8]J. Mizuguchi, Ber. Bunsenges. Phys. Chem. **97**, 684 (1993).
[9]J. M. Ziman, *Principles of the Theory of Solids*, 2nd ed. (Cambridge University Press, Cambridge, 1972).
[10]K. Seeger, *Semiconductor Physics*, 3rd ed. (Springer-Verlag, Berlin, 1985).
[11]A. C. Rochat, L. Cassar, and A. Iqbal, U.S. Patent No. 4,579,949 (filed May 11, 1986).
[12]J. Mizuguchi, Krist. Tech. **16**, 695 (1981).
[13]J. Mizuguchi, T. Imoda, H. Takahashi, and H. Yamakami, Dyes Pigm. **68**, 47 (2005).
[14]Quantum CACHE Ver. 3.2, Fujitsu Ltd. (1999).
[15]J. Mizuguchi, J. Phys. Chem. A **104**, 1817 (2000).